1.0

4.5
5.0
5.6
6.3

2.8

2.5

3.2

2.2

3.6

1.1

4.0

2.0

1.8

1.25

1.4

1.6

MICROCOPY RESOLUTION TEST CHART

NATIONAL BUREAU OF STANDARDS-1963-A

AD A063823

LEVEL

RADC-TR-78-162
Final Technical Report
July 1978

CONTOUR MAPPING OF DETECTOR ARRAYS

D. P. Mathur

The Perkin-Elmer Corporation

DDC
RECEIVED
JAN 26 1979
C

Approved for public release, distribution unlimited

ROME AIR DEVELOPMENT CENTER
Air Force Systems Command
Griffiss Air Force Base, New York   13441

79 01 26 014

This report has been reviewed by the RADC Information Office (OI) and is releasable to the National Technical Information Service (NTIS). At NTIS it will be releasable to the general public, including foreign nations.

RADC-TR-78-162 has been reviewed and is approved for publication.

APPROVED: *Jerry Silverman*

JERRY SILVERMAN
Project Engineer

APPROVED: *Clarence D. Turner for*

ROBERT M. BARRETT, Director
Solid State Sciences Division

FOR THE COMMANDER: *John P. Huss*

JOHN P. HUSS
Acting Chief, Plans Office

If your address has changed or if you wish to be removed from the RADC mailing list, or if the addressee is no longer employed by your organization, please notify RADC (ESE) Hanscom AFB MA 01731. This will assist us in maintaining a current mailing list.

Do not return this copy. Retain or destroy.

(19) REPORT DOCUMENTATION PAGE		READ INSTRUCTIONS BEFORE COMPLETING FORM
1. REPORT NUMBER (18) RADC-TR-78-162	2. GOVT ACCESSION NO.	3. RECIPIENT'S CATALOG NUMBER
4. TITLE *(and Subtitle)* (6) CONTOUR MAPPING OF DETECTOR ARRAYS.	(9)	5. TYPE OF REPORT & PERIOD COVERED Final Technical Report. Mar 1977 to Jul 1978
		6. PERFORMING ORG. REPORT NUMBER (14) PE-13448-2
7. AUTHOR(s) (10) D. P. Mathur	(15)	8. CONTRACT OR GRANT NUMBER(s) F19628-77-C-0129
9. PERFORMING ORGANIZATION NAME AND ADDRESS The Perkin-Elmer Corporation Norwalk, CT 06852	(16)	10. PROGRAM ELEMENT, PROJECT, TASK AREA & WORK UNIT NUMBERS 61101F 1L1R0021 (17) PP
11. CONTROLLING OFFICE NAME AND ADDRESS Deputy for Electronic Technology (RADC/ESE) (11) Hanscom AFB MA 01731 Monitor/Jacques E. Ludman/ESE		12. REPORT DATE July 1978
		13. NUMBER OF PAGES 88 (12) 89 p.
14. MONITORING AGENCY NAME & ADDRESS(if different from Controlling Office) Same		15. SECURITY CLASS. (of this report) UNCLASSIFIED
		15a. DECLASSIFICATION/DOWNGRADING SCHEDULE

16. DISTRIBUTION STATEMENT *(of this Report)*

Approved for public release; distribution unlimited

17. DISTRIBUTION STATEMENT *(of the abstract entered in Block 20, if different from Report)*

Same

18. SUPPLEMENTARY NOTES

RADC Project Engineer: Jerry Silverman (ESE)
This research was supported by the Air Force In-House Laboratory Independent Research Fund.

19. KEY WORDS *(Continue on reverse side if necessary and identify by block number)*

Contour Mapping
Detector Responsivity
Extrinsic Silicon Detectors
Detector Contact Evaluation

20. ABSTRACT *(Continue on reverse side if necessary and identify by block number)*

The anomalous behavior of the extrinsic silicon infrared detectors operating at very low temperatures under very low background photon-flux conditions has been extensively reported. A recent theoretical investigation of Ludman and Silverman addressed the anomalous behavior of these detectors near the contact region. The ohmic contacts to these silicon detectors can be considered as high-low junction contacts. The theory then investigates the variations in the detector responsivity near the contacts in view of the effects at low temperature of the high-low junction contacts. (Con'td)

DD FORM 1 JAN 73 1473   EDITION OF 1 NOV 65 IS OBSOLETE

UNCLASSIFIED over

279 550

79 01 26 014

This report describes the results of measurements of responsivity of extrinsic silicon infrared detectors near their ohmic contacts. These detector responsivity measurements were made by utilizing an apparatus developed at The Perkin-Elmer Corporation. This apparatus consists of a source of infrared radiation focused to a spot and mounted on a cryogenic x-y stage. The source of radiation and the cryogenic stage are mounted in the same low background photon flux and low temperature chamber as the detectors. The description of the apparatus and its characterization are also presented in this report.

The responsivity of these detectors near the contacts deconvolved with the dimensions of the experimental focused spot indicated the extent (distance) to which the contacts alter the equilibrium conditions in the bulk semiconductor. Clearly, the contact effects are dependent on the background photon-flux on the detectors. Hence, the detectors responsivities were measured under high and low background photon-flux conditions. The results of these measurements in view of the theoretical predictions are also reported here.

The experimental effort reported here should be examined as a very preliminary step towards understanding or experimentally establish some of the predicted abnormal behavior of extrinsic silicon infrared detectors. However, some general conclusions can be derived on the basis of this work and are listed below:

1. Contact Effects - Revisions in application of Ludman/Silverman Theory* to SiAs after the contract was initiated showed the effects to be milder by a factor of ten than originally believed. Hence, we were looking for contact effects extending to 2 μm with a 70 μm spot. Given other non-ideal effects (surface states, defects, etc.) expected near the contact region, it is not surprising that no enhancement at the contacts was found. When this was realized, emphasis shifted to establish contour reproducibility. In particular, whether true, "lifetime profile" is measured in this type of anode to cathode scan.

2. Some confidence in the reproducibility of contours has been established with a range of scan rate, chopping frequency and laser power.

3. Better or sharper detector contacts are required to obtain accurate measurements of the contact effects--perhaps ion implanted n^+ contacts. A uniform detector response between the contacts will help the data analysis immensely. A small spot size adds to the accuracy of measurements.

4. Utilize detectors which have higher operating temperatures for which higher enhancement in responsivity due to carrier "spill-over" is expected.**

---

* Private Communication - Ludman/Silverman
** Private Communication - Ludman/Silverman

EVALUATION

1. This report is the Final Report on the contract. It covers
research done on characterization of responsivity profiles of low
compensation extrinsic silicon arsenic infrared detectors by scanning
with a seventy micron spot of laser light. A realm of conditions
(laser power, chopping frequency, scan speed and background level)
was identified where a true responsivity contour is observed.
Recommendations were made on modified experiments in order to
definitively test a theory of contact effects developed at LT.

2. The above work is of value in providing guidance as to the proper
characterization and testing of IR detectors already used in and
planned for USAF surveillance systems.

Jerry Silverman
JERRY SILVERMAN
Project Engineer

iii

TABLE OF CONTENTS

LIST OF TABLES

LIST OF ILLUSTRATIONS

LIST OF ILLUSTRATIONS

SECTION I

1.1 INTRODUCTION

The anomalous behavior of the extrinsic silicon infrared detectors operating at very low temperatures under very low background photon-flux conditions has been extensively reported. A recent theoretical investigation of Ludman and Silverman addressed the anomalous behavior of these detectors near the contact region. The ohmic contacts to these silicon detectors can be considered as high-low junction contacts. The theory then investigates the variations in the detector responsivity near the contacts in view of the effects at low temperature of the high-low junction contacts. The profiles of the free-carriers and ionized impurity concentrations can be obtained by considering the contacts as a one-dimensional abrupt junction. The bulk material, considered as the low side of the junction, is assumed to have a doping level of 10^{16} impurities/cm^3 and compensation levels in the range of 10^{12} to 10^{14} carriers/cm^3. Order of magnitude perturbations from bulk equilibrium carrier concentrations are predicted on the low side of the junctions of distances up to 5μm from the junction interface or the contacts. The effect of these perturbations in carrier concentration might experimentally be realized by measuring the response of the detectors to infrared radiation as a function of the distance from the contacts.

This report describes the results of measurements of responsivity of extrinsic silicon infrared detectors near their ohmic contacts. These detector responsivity measurements were made by utilizing an apparatus developed at The Perkin-Elmer Corporation. This apparatus consists of a source of infrared radiation focused to a spot and mounted on a cryo-

1

genic x-y stage. The source of radiation and the cryogenic stage are mounted in the same low background photon flux and low temperature chamber as the detectors. The description of the apparatus and its characterization are also presented in this report.

The responsivity of these detectors near the contacts deconvolved with the dimensions of the experimental focused spot indicated the extent (distance) to which the contacts alter the equilibrium conditions in the bulk semiconductor. Clearly, the contact effects are dependent on the background photon-flux on the detectors. Hence, the detectors responsivities were measured under high and low background photon-flux conditions. The results of these measurements in view of the theoretical predictions are also reported here.

1.2 PROGRAM OBJECTIVES

The objectives of this program were to measure the detector responsivity by scanning a focused spot of infrared radiation across the active area of the detector under the following conditions.

a. Various intensities of the focused spot.

b. Various scanning speeds of the focused spot.

c. Various modulation frequencies of the focused spot.

d. The above experiments repeated for higher background photon-flux conditions.

The other objective of this program was to analyze the results in terms of the predicted theory.

SECTION II

CONTOUR MAPPING APPARATUS

2.1 INTRODUCTION

The low temperature and low background photon-flux apparatus for measuring spatial responsivity of infrared detectors was developed by Perkin-Elmer under IR&D funding. The responsivity contour mapping apparatus is a part of a sample holder for the variable temperature liquid helium cryostat. Photographs of the cryostat and the sample holder are shown in Figure 1. The contour mapping apparatus is briefly described in the following paragraph.

2.2 GENERAL DESCRIPTION OF THE CONTOUR MAPPING APPARATUS

A schematic drawing of the contour mapping apparatus is shown in Figure 2. The apparatus consists of a lead-tin-selenide laser diode which is the source of the infrared radiation at 10.6 μm. The radiation from the laser diode overfills a 200 μm diameter aperture. A single f/2.5 germanium lens is placed so as to demagnify the aperture by a factor of 8. A schematic diagram of the laser diode and the lens is shown in Figure 3. A photograph of the laser-lens mount is shown in Figure 4. This mount is designed to eliminate any stray infrared radiation, and hence, allows changing the laser radiation output by many orders of magnitude without changing the background photon-flux conditions. The laser-lens mount is attached to the x-y cryogenic stage. The detectors under test are mounted in a plane perpendicular to the optical axis of the optical axis of the laser-lens mount. The detectors, laser-lens mount and the x-y stage are enclosed in a copper container with blackened walls which, being at a temperature of 4.2°K, provide the very-low background photon flux conditions.

The cryogenic stage is driven by geared down dc motors external to the helium cryostat. These motors also drive ten-turn potentiometers

which serve as the x and y position sensors for the cryogenic stage. The detector output signal together with the outputs of the x and y position sensors are fed to an x-y recorder via an adapter circuit to obtain pseudo three dimensional plots of detector responsivity as a function of position of the focused spot. A schematic diagram of the electrical circuits for the contour mapping apparatus is shown in Figure 5. The infrared radiation is modulated by controlling the current through the laser diode at the desired frequency. The details of the adapter circuit for the x-y recorder are described below.

2.3 ADAPTER CIRCUIT FOR X-Y RECORDER

An adapter circuit was designed and built to modify the x-y recorder output to obtain the perspective three-dimensional plot. The basic principle of this adapter circuit is shown in Figure 6, and Figure 7 shows the detail schematic of the adapter circuit. In Figure 6, X IN and Y IN are the voltages from the x and y position sensors of the cryogenic stage. Adjustable portions of X IN and Y IN, and the detector output signal (denoted, respectively, by a b and c in Figure 6), are fed into the two operational amplifiers to obtain the psuedo-three-dimensional effect. A full range d.c. offset for both x and y axes was incorporated in the adapter circuit so that any portion of the scan could be appropriately expanded. A signal simulator was also built into the adapter circuit to test the three-dimensional plots and thereby provide a reference. Figure 8 shows a three-dimensional plot obtained by using the adpater circuit and the signal simulator.

2.4 CHARACTERIZATION OF THE FOCUSED LASER SPOT

To understand the results of contour-mapping an infrared detector, it is important to define the diameter and the profile of the focused spot. The approach taken here to characterize the spot was to focus the spot at a pinhole, 25μm in diameter, in a metal mask placed in close proximity to a large (2mm by 1mm) extrinsic silicon detector. The focused spot was scanned past the pinhole and the detector signal versus the position of the spot was recorded. Mathematically, scanning the spot across the pinhole and collect-

4

ing all the energy passing through the pinhole represents a convolution of the focused laser spot with the pinhole in the mask. Thus, the shape and size of the focused laser spot can be obtained by deconvolving the experimentally determined values of the detector signal with the circular pinhole. To a first approximation the diameter of the spot alone can be obtained by subtracting 25μm, the diameter of the pinhole, from the diameter of the experimentally determined detector signals. The results of the pinhole experiments are shown in Figure 9 which shows that the focused spot is very symmetrical. The diameter of the circle defined by the points, where the signal goes to zero from Figure 12, is 95μm. As mentioned above, the diameter of the spot to a first approximation is obtained by subtracting 25μm from the measured diameter of 95μm, and is 70μm.

In the contour-mapping apparatus, the radiation from a 10.6μm laser diode is focused to a spot by a single f/2.5 germanium lens. The diameter of the first dark ring of a diffraction-limited spot is given by

$$\text{diameter (in μm)} = 2.44 \, \lambda f/\text{No.}$$

where λ is in μm which for the present case is 10.6μm. Thus the diameter of the first dark ring is 65μm. This agrees remarkably well with the measured value.

The scan was continued to 0.1 inch in both x and y directions from the pinhole, and no signal was observed within the experimental error, which was ±2% of the peak signal. Thus, we concluded that there are neither measurable side lobes of the spot or any unwanted reflections. The jagged appearance of the contours in Figure 12 is due to the finite steps in the position sensors of the x-y cryogenic stage. Each of the regularly spaced jagged steps corresponds to 2.5μm, which is also the limit of accuracy of our apparatus. It appears that we have a near diffraction-limited, symmetrically focused laser spot with a diameter of 70μm inch at the detector and with no measurable side-lobe configurations.

2.5 BACKGROUND PHOTON-FLUX MEASUREMENTS

An arsenic-doped silicon detector, calibrated by the Naval Electronics Laboratory Center at San Diego, was installed in the same plane as the detec-

tor arrays under test.   The calibration data on this background photon-flux monitor detector is shown in Figures 10 and 11.   The impedance of the monitor detector was directly measured by using a Keithley Model 610 electrometer. The measured impedance was 3×10^{13}ohms, which from Figure 13 corresponds to ~3×10^9 photons/sec cm^2 at 2.5μm or $\sim10^9$ photons/sec cm^2 at 10.6μm using the spectral calibration curve shown in Figure 10.   The impedance of this detector was measured during different experiments for various laser output powers and positions and was found to be the same within experimental error.
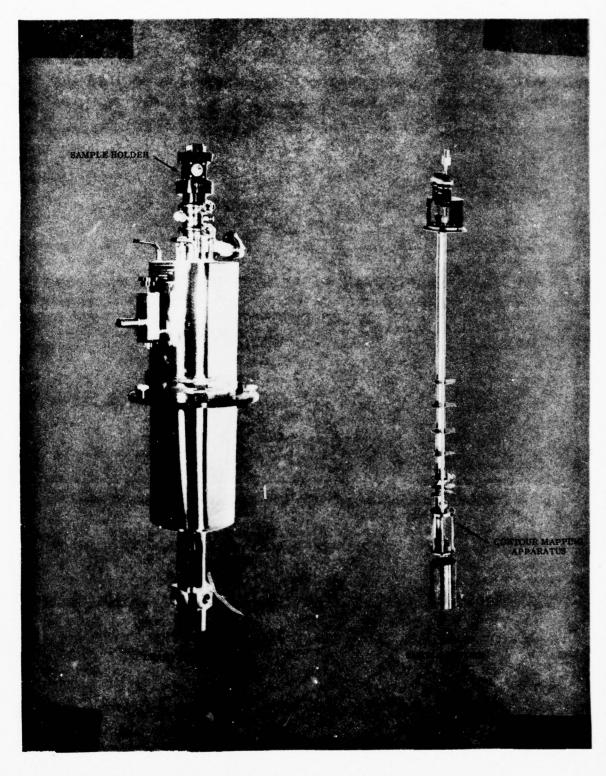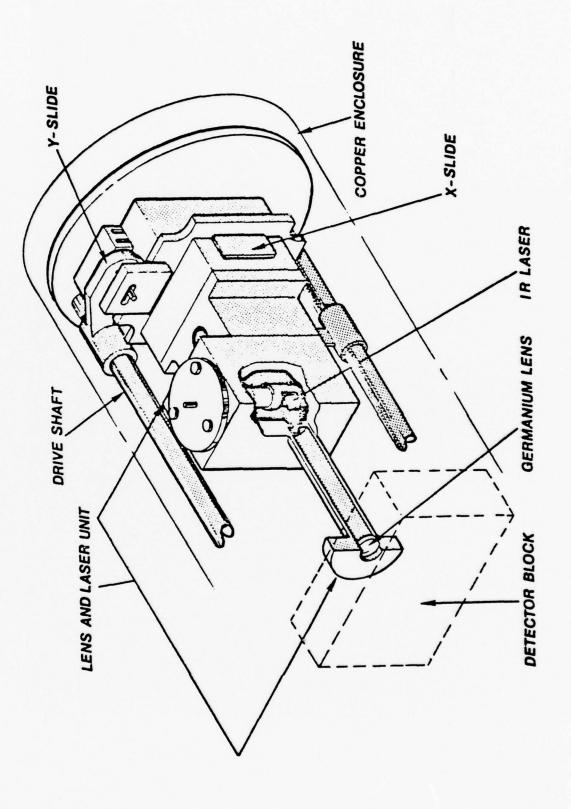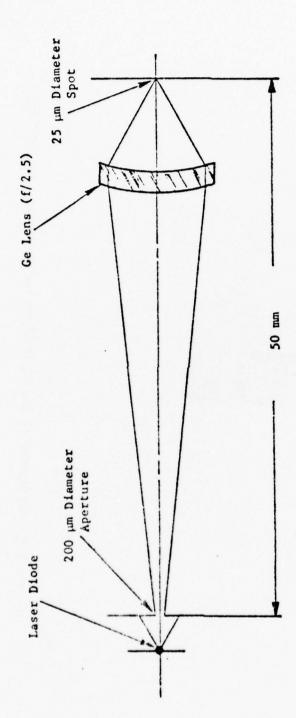
Figure 2.1. Sample Holder and the Liquid Helium Dewar for the
Contour Mapping Apparatus

7

Figure 2.2. Schematic Drawing of the Perkin-Elmer Contour Mapping Apparatus

Figure 2.3. Schematic Drawing of the 10.6μm Laser Diode Source and the Germanium (f/2.5) Lens

9
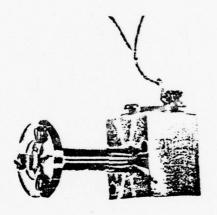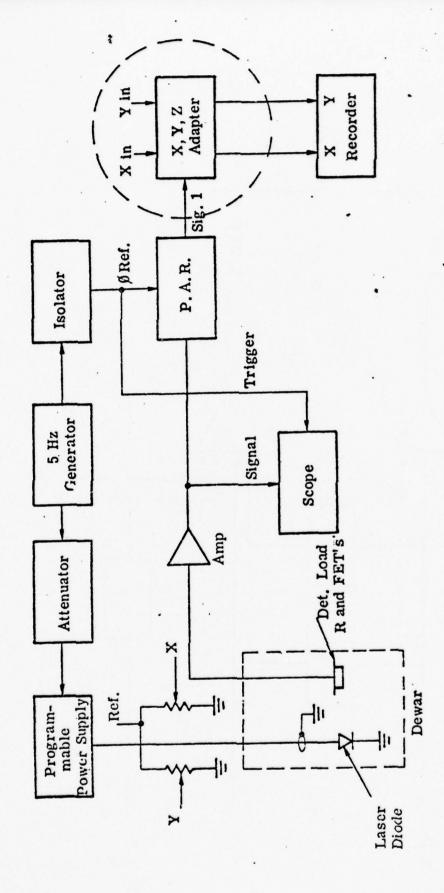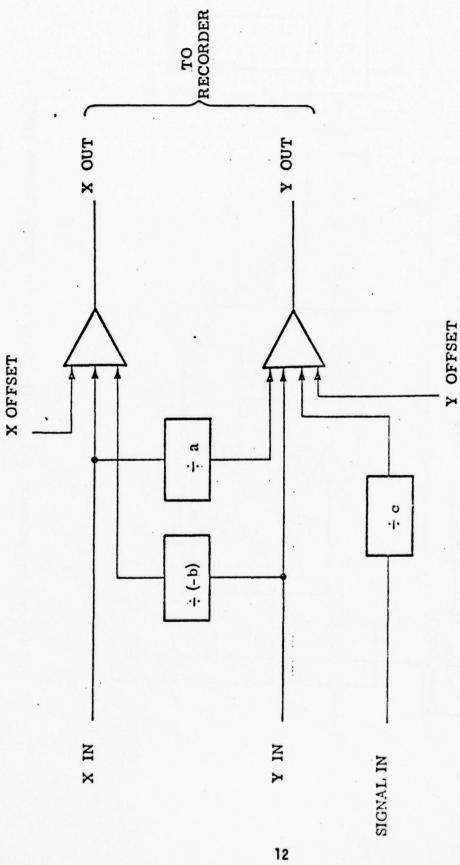
Figure 2.4. Photograph of the Laser Diode and Germanium Lens Assembly

Figure 2.5. Schematic of Electronic Circuitry for Contour Mapping Apparatus

11

Figure 2.6. Block Diagram of the x-y-z Adapter Circuit to Obtain Pseudo Three Dimensional Responsivity Contour Plots

12
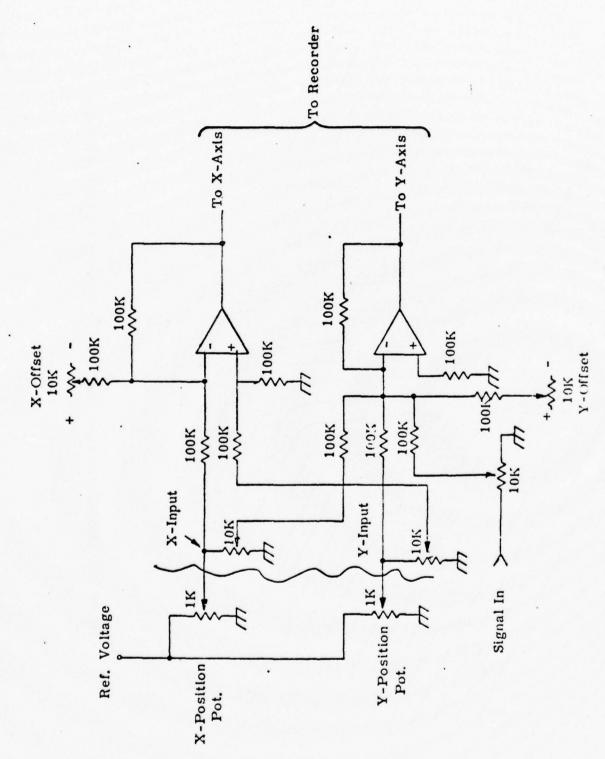
Figure 2.7. Schematic Diagram of the x-y-z Adapter Circuit

13

SIGNAL

X

Y
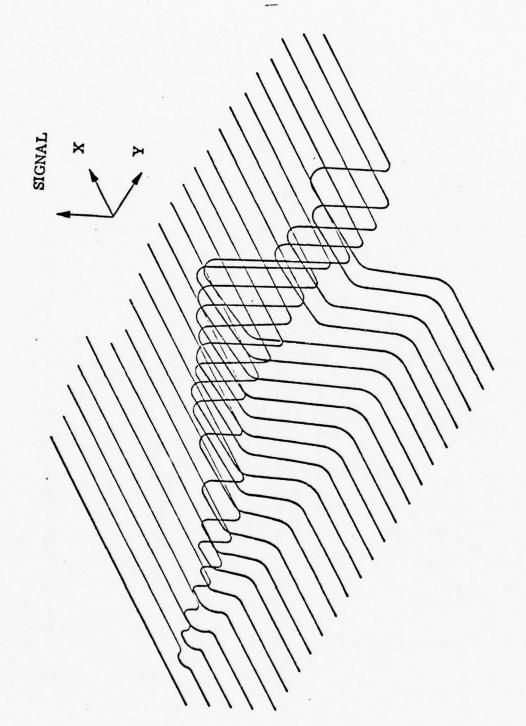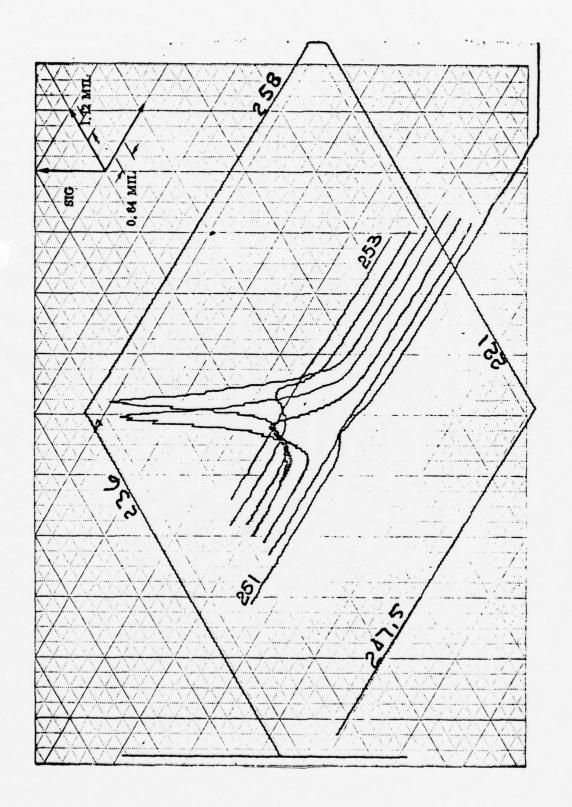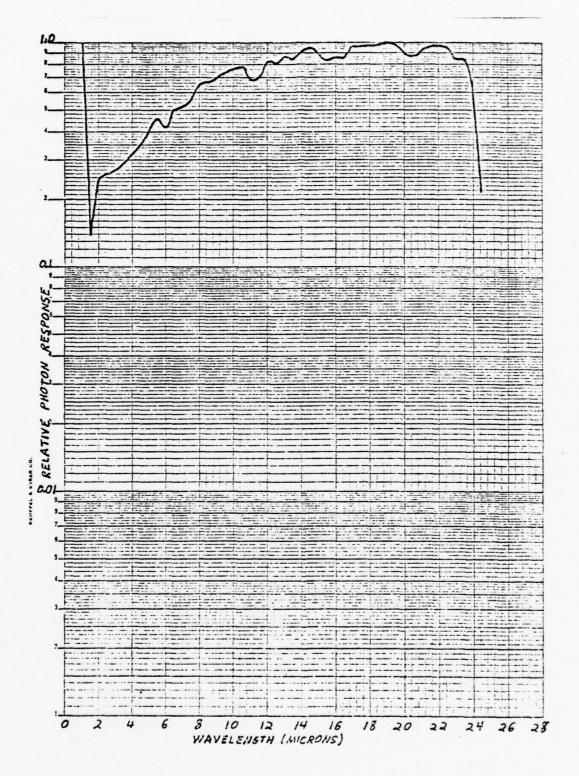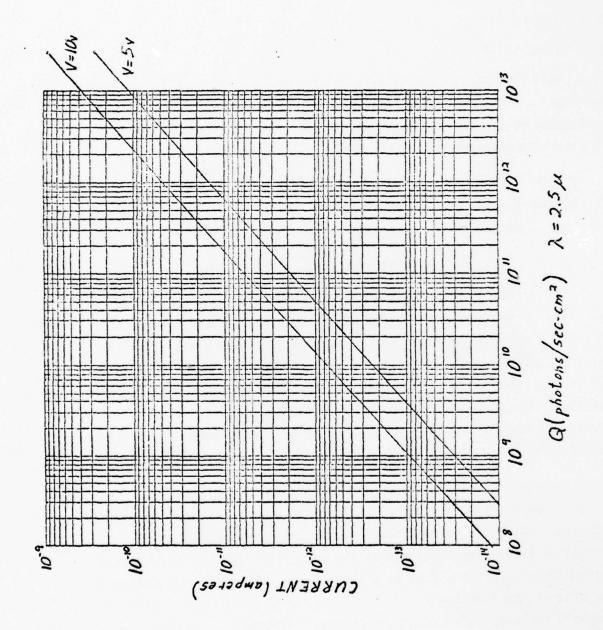
Figure 2.8. A Simulated x-y-z Plot Obtained by Using the Adapter Circuit

14

Figure 2.9. Results of Scanning a 0.001-inch Hole Mask with Focused Laser Beam – Symmetrical Focused Spot

Figure 2.10. Relative Spectral Response of the Background Monitoring Detector as Supplied by NELC

Figure 2.11.   Current vs. Background Photon Flux (Q_B) at 5V and 10V Bias for the Background Photon-Flux Monitoring Detector at $\lambda \cong 2.5\mu$ (data supplied by NELC)

17

SECTION III

SUMMARY OF THEORETICAL PREDICTIONS

3.1 INTRODUCTION

This section summarizes very briefly the predictions of Ludman and Silverman's theory on the high-low junction contacts. The theoretical prediction of highest interest for this work is the enhanced detector responsivity near the contacts.

This section also summarizes the effects of the finite size of the experimental focused spot used to investigate the region of enhanced responsivity.

3.2 SUMMARY OF HIGH-LOW JUNCTION THEORY

The effect of high-low contacts to extrinsic silicon infrared detectors at low temperatures has been theoretically investigated. The effect has been studied for the case of zero bias electric field The profiles of the free-carriers and ionized impurity concentrations can be obtained by considering the contacts as a one-dimensional abrupt junction. The bulk material, considered as the low side of the junction, is assumed to have a doping level, N_D, of 10^{16} impurities/cm^3 and compensation levels, N_A, in the range of 10^{12} to 10^{14} carriers/cm^3.

Figure 3.1 shows a plot of the ionized donor profiles, N_D^+ high-low junction in thermal equilibrium as a function of distance from the contacts at several compensation levels. The n^+n junction is assumed to be 10^{19} to 10^{16}. As can be seen from Figure 3.1, orders of magnitude perturbations from bulk equilibrium values are observed on the low side of the junction up to 3 microns. This "spill-over" effect into the bulk semiconductor results in enhanced lifetime and hence detector

responsivity near the contacts. The predicted "point" responsivity as a function of distance from the contacts is listed in Table 3.1. The effect of these perturbations in carrier concentration can be experimentally realized by measuring the response of the detectors to infrared radiation as a function of the distance from the contacts.

Thus for n-type infrared silicon detectors with $N_D \sim 10^{16}$ in the bulk region and a compensation level, N_A, of 5×10^{12} with an n^+ contact (10^{19} carriers/cc) theory predicts

- o Carrier spill-over

- o Ionized donor depletion effects

- o Resulting in life-time and hence responsivity enhancement up to $3\mu m$ from the contacts.

3.3 EFFECT OF EXPERIMENTAL FOCUSED SPOT

The theory indicates that the contact effects on the detector responsivity should happen in the first $3\mu m$ or so. The question arises whether one can see an effect confined to $3\mu m$ from the contacts with our scanning spot which is $70\mu m$ in diameter (as shown in Section II).

A theoretical analysis was conducted to establish the effect of our experimental spot convolved with:

a. Ideal response of an ideal detector (with no contact-effects).

b. Response of an ideal detector with enhanced responsivity near the contacts.

Figure 3.2 shows the ideal response of an ideal detector and the predicted profile when convolved with our experimental spot. Figure 3.3 shows the results of calculations for the case of a detector with contact enhanced spikes convolved with our experimental spot.

Figures 3.3(a), 3.3(b), 3.3(c) and 3.3(d) show the results of enhanced responsivity of 10^5, 888, 40 and 3.1 respectively. In these results note the following:

o   The curves marked "ideal" show the effect of contacts on a detector scanned with a point spot.

o   The curves marked "measured" show the corresponding profiles when convolved with our experimental spot. The curves marked "measured" also show the effect for one contact only for the sake of simplicity. The distance scales of the corresponding profiles have been arbitrarily displaced.

For these "measured" curves, the enhanced responsivity at the contacts is clearly discernable for the first three cases. However, for the enhancement of 3.1 in responsivity the "measured" curve does not have the clearly defined "bump" at the contact. Figure 3.4 shows the case of 3.1 enhanced responsivity redrawn on a larger scale. Also shown in the "measured" curve for the case of no contact effects. It is evident in Figure 3.3 that the slope of the curve for 3.1 responsivity enhancement is higher than that for no contact effects, and is about a factor two higher. This tends to indicate that enhancement effects as low as 3.1 might be experimentally measured with our focused spot.

3.4   EXPERIMENTAL RATIONALE

Based upon the above, the following situations could occur in actual detectors: (a) the enhanced responsivity is $\geq$ 40, hence large responsivity peaks at the detector edges, (b) the enhanced responsivity is $\leq$ <40 so that there is no discernable responsivity peak at the edges of the detectors. Thus the logical approach to study the contact effects is to conduct the experiments in the following order:

1.   Measure the responsivity of the detector as the focused spot transverses from contact to contact or parallel to the bias direction. If a peak in the responsivity is observed near the detector edges then condition (a),

described above, is applicable. If no responsivity peak is observed, then condition (b) is applicable.

2. If condition (b) is applicable then measure the respon-sivity by scanning the focused spot parallel and per-pendicular to the bias field. The scan perpendicular to the bias field produces a situation of no contact effect. Thus the difference in slopes of the scans parallel and perpendicular to the bias field, if any, will give the magnitude of the enhanced responsivity.

3. Measure the responsivity under very low background photo-flux on the detector and repeat the measurement by increasing the background photon flux by many orders in magnitude. The latter high background photon-flux condition might minimize the contact effects condition and thus providing the required reference (no effect) condition.

The results of these experiments are described in Section IV.
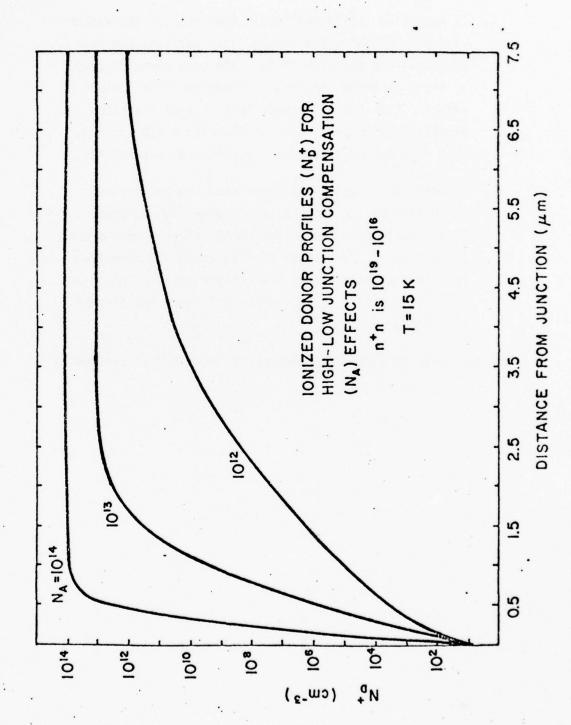
FIGURE 3.1 Electron 'spill-over' as a function of distance from contact for different N_A.
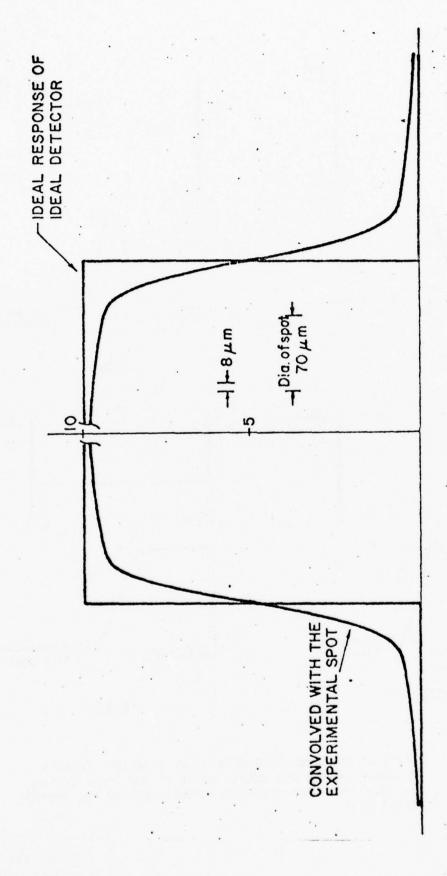
Figure 3.2. Response of an Ideal Detector and Result of Convolution with the Experimental Spot
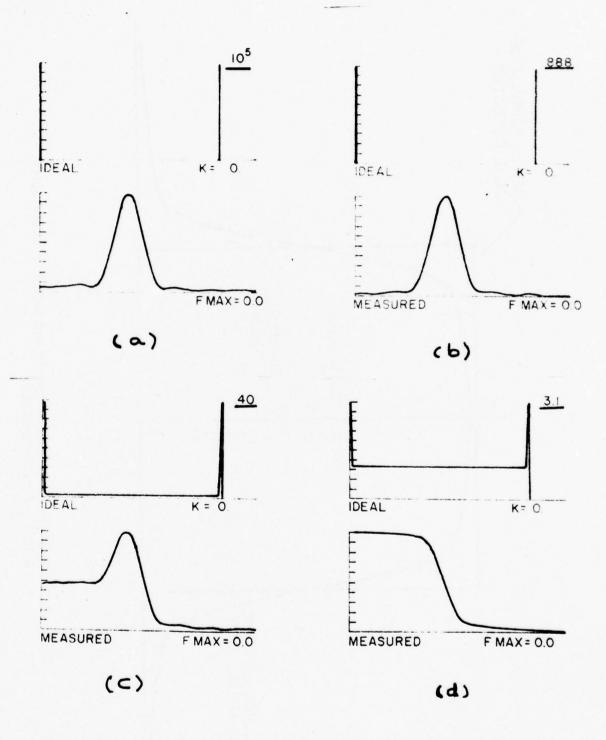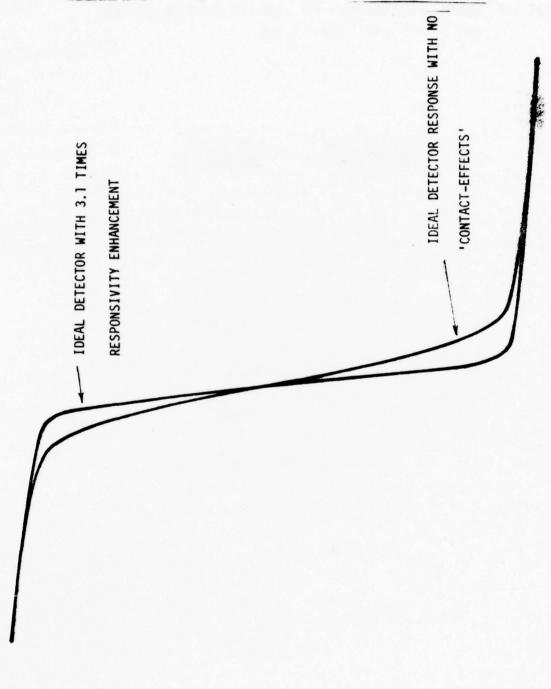
Figure 3.3. Effect of Enhanced Responsivity at Detector Contacts-- the upper curves are ideal responses and lower curves are ideal detector responses convolved with our experimental spot

24

TABLE 1.3 ENHANCED RESPONSIVITY FOR HIGH-LOW JUNCTION CONTACTS
WITH $N_A = 5 \times 10^{12}$ AND T = 15K

Position From Contact (μm)	Enhanced Responsivity
0	∞
0.5	∞
1.0	∞
2.1	7×10^{10}
2.37	2.5×10^5
2.7	880
3.3	3.1

IDEAL DETECTOR WITH 3.1 TIMES
RESPONSIVITY ENHANCEMENT

IDEAL DETECTOR RESPONSE WITH NO
'CONTACT-EFFECTS'

Figure 3.4. Comparison of Spot-Convolved Detector Responses for the Cases of 3.1 Times Enhanced Responsivity and with Zero Enhanced Responsivity

26

SECTION IV

RESULTS

4.1 INTRODUCTION

This section describes the results of responsivity scans conducted on three extrinsic silicon detectors under different measurement conditions.

4.2 CHARACTERISTICS OF DETECTORS INVESTIGATED

The work conducted during this reporting period was performed on three extrinsic silicon detectors, two supplied by Hughes Research Laboratory and one supplied by Rockwell International. The characteristics of these three detectors are summarized in Table 4.1.

TABLE 4.1. DETECTORS MEASURED

Type of Contract: N^+N

Source	Impurity	N_D	N_A
Rockwell Int.	Si:As	$\sim 10^{16}$	$\sim 1 \times 10^{13}$
Hughes Res. Lab	Si-As	$\sim 10^{16}$	$\sim 2 \times 10^{13}$

4.3 DETECTOR-AMPLIFIER ASSEMBLY

The detectors were mounted on a common substrate, and along with the preamplifiers and the total assembly in turn was mounted to a copper block. The detector-preamplifier package configuration is schematically shown in Figure 4.1 The design of the lead-out pattern on the substrate allowed the direction of detection bias to be easily changed during test measurements.

The detector-preamplifier package was installed in the cryostat containing the contour mapping facility.

4.4 MEASUREMENT RESULTS

Detector responsivity contours were mapped to establish a reasonably good detector area to be used for the study of contact effects. Some of these pseudo three-dimensional contour maps are shown in Figures 4.2 and 4.3. These measurements indicated that there were no areas of the detectors which presented a uniform responsivity contour. These experiments also showed that the two detectors supplied by Hughes Research Laboratory (Figure 4.2) behaved very similar to each other and appeared to be more uniform than the Rockwell International detector (Figure 4.3).

Responsivity contour maps of Hughes detectors are shown in Figures 4.4 and 4.6. These scans parallel to the bias field, show that

a. The detectors are not uniform.

b. At the contacts, the responsivity does not show peaks consistent with condition (a) (see Section 3.4).

The above responsivity contour maps of Hughes detectors were repeated with the bias field reversed. This scan is shown in Figure 4.7. The shape of the responsivity scan shown in Figure 4.7 is different than those of Figure 4.4 to 4.6, possibly due to a shift in detector area scanned. However, if the reverse-biased scan (Figure 4.7) is superimposed on one of the parallel scans (Figure 4.4), we find that the initial slope of the scan is the same (see Figure 4.8). This result should be considered only as a preliminary evidence and does not conclusively prove that the direction of the bias field has no effect on the detector responsivity contour.

In the absence of any responsivity peaks near the contacts of these detectors, we measured the responsivity contour maps of the detectors parallel to the bias field and perpendicular to the bias field. The scan perpendicular to the bias field provides the case of no contact effects and is shown in Figure 4.9. The slopes of the beginning of the responsivity contour maps of Figure 4.4 (parallel scan) and Figure 4.9

28

(perpendicular scan) are shown in Table 4.2. Table 4.2 also shows the
slopes of the responsivity contours of the theoretical non-contact
effect and contact-effect case as shown in Figure 3. of Section III.
The slope of the contour with no contact effects was higher than that for
the one that contained contact effects. This is clearly contrary to
the expected result. In order to understand this anomalous behavior,
it was suggested (Ludman and Silverman) that we conduct the following
experiments: Turn the focused spot on and off while it is focused at
the same point on the detector and measure the time it takes for the
signal to rise or fall. The results of these experiments are shown
in Figures 4.10 and 4.11 and show that the signal rises with a time
constant of several seconds when the laser radiation is turned on.
The scan rate was approximately 10μm/sec.

This modified scanning technique suggests that if the contour
mapping was done at a scan rate faster than the time it took for the
signal to rise, then the effects due to the contacts would be totally
masked. In view of this discovery a list of suitable experimental
conditions was developed. The list of the experiments is as follows:

Experiment No. 1

a. Intensity of the focused-spot constant (or laser current
at 300ma and constant).

b. Spot scan speed fixed at the lowest value possible.

c. Three different laser modulation frequencies, namely,
1.5Hz, 5Hz and 10Hz.

d. Repeat (c) for two higher scan rates.

e. Repeat at least one or two of the above nine scans to
show reproducibility.

f. Laser on-off experiments at three points on the detector,
namely, anode, cathode and the center of the detector.

29

TABLE 4.2. SLOPES OF THE BEGINNING OF THE CONTOURS

Experiment	Slope
Perpendicular Scan	2.02 (63.8°)
Parallel Scan	1.43 (55°)
Theoretical No Contact Effect	1.43 (55°)
Theoretical with Contact Effect (3.1 times)	6.35 (81.1°)

TABLE 4.3. LIST OF SCANS FOR EXPERIMENTS NO. 1 AND NO. 2

(Low Background)

Figure No	Laser Freq. in Hz	Laser Power ma	Scan Rate μm/sec	Slope of the Scan in Deg.
4.12, 4.13	1.5	300	4.25	83
4.14, 4.15	.5	300	4.25	85
4.16	10	300	4.25	81
4.17	1.5	300	5.5	82.5
4.18	1.5	300	7.0	84
4.19	5.0	300	5.5	84.5
4.20	5.0	300	7.0	84
4.21	10	300	5.5	82
4.22	10	300	7.0	81
4.23, 4.24	5	500	5.5	84
4.25, 4.26	5	100	5.5	83
4.27	5	550	5.5	80
4.28, 4.29	5	400	Discrete	84
4.30, 4.31, 4.32	5	400	Laser on-off	

TABLE 4.4.   LIST OF SCANS FOR EXPERIMENT NO. 3

(High Background)

Figure No.	Laser Freq. in Hz	Laser Power Amp	Scan Rate μm/sec.	Slope of the Scan in Deg.
4.33	1.5	1	5.5	77
4.34	1.5	1	5.5	81
4.35	1.5	1	7.0	80
4.36	5	1	4.25	81
4.37	5	1	5.5	81
4.38	5	1	5.5	81
4.39	5	1	7.0	82
4.40	10	1	4.25	82
4.41	10	1	5.5	82
4.42	10	1	7.0	83
4.43	5	1	5.5	82
4.44	5	1	5.5	82

Experiment No. 2

   a. Scans at the best scan rate and modulation frequency, as
       determined by Experiment No. 1, for three different laser
       powers.

   b. If possible, at one laser power do a discrete scan which is
       essentially driving a spot to a position and stopping the
       scan and so on.

Experiment No. 3

   a. Repeat Experiment No. 1 for the case of high background
       photon flux conditions.

   Experimentally, the lowest scan rate was found to be 4.25μm/sec.
Below this scan rate large sticktion in the gear drive was observed.
The variables for the above three experiments are listed in Table 4.3 and
4.4.

4.4.1 Results of Experiments No. 1 and No. 2

   Figures 4.12 to 4.32 show the results of Experiments No. 1 and
No. 2. The different measurement conditions for scans shown in Figures
4.12 to 4.32 are listed in Table 4.3. Table 4.3 also list the slope of
the initial part of each scan in degrees. Figures 4.30, 4.31 and 4.32
show the results of the laser on-off experiment with the focused spot at
the anode, the center of the detector and the cathode respectively. The
time constant for the signal to reach 1/e of its maximum value when
the laser was turned on was 1.2 secs and was the same for all three
positions. The signal fall time when the laser was turned off was
0.3 sec in all three cases. Figures 4.28 and 4.29 show the results
of discrete scan. At each of the positions masked, the scan was
stopped for 10 secs. These scans showed nothing different from all
the other scans.

4.4.2 Results of Experiment No. 3

   The results of Experiment No. 3 are shown in Figures 4.33 to
4.42. The different measurement conditions for scans shown in

Figures 4.32 to 4.42 are listed in Table 4.4. As the results of
these scans taken under high background photon-flux conditions, the
detector signal to noise is considerably higher and thus results
in poor quality of the responsivity contour maps.
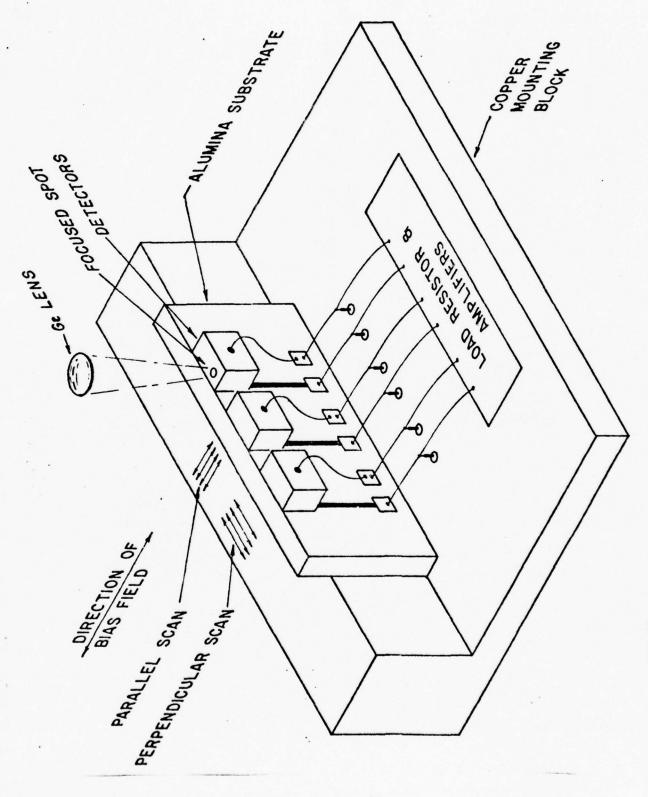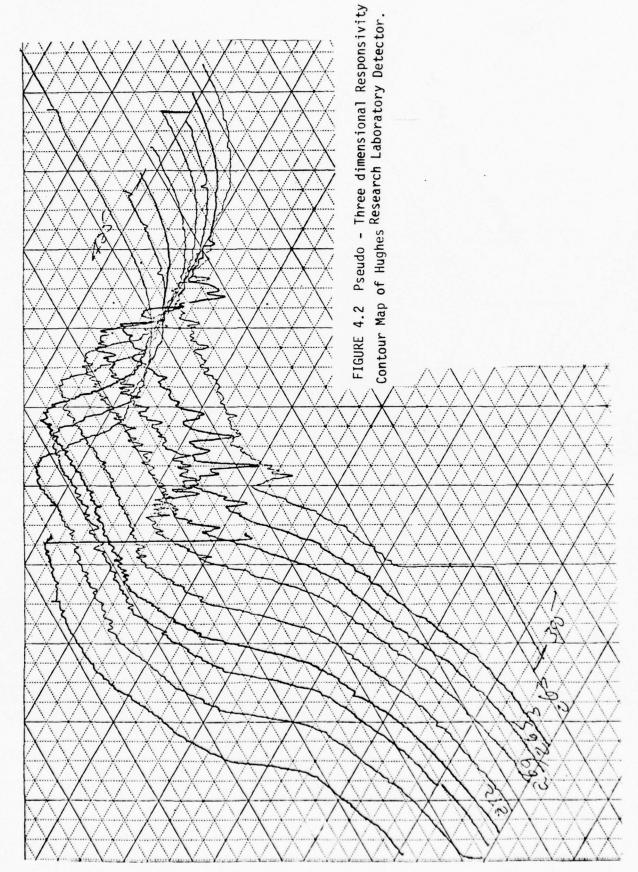
FIGURE 4.1 Schematic of the Experimental Configuration.

35

FIGURE 4.2 Pseudo - Three dimensional Responsivity
Contour Map of Hughes Research Laboratory Detector.

36
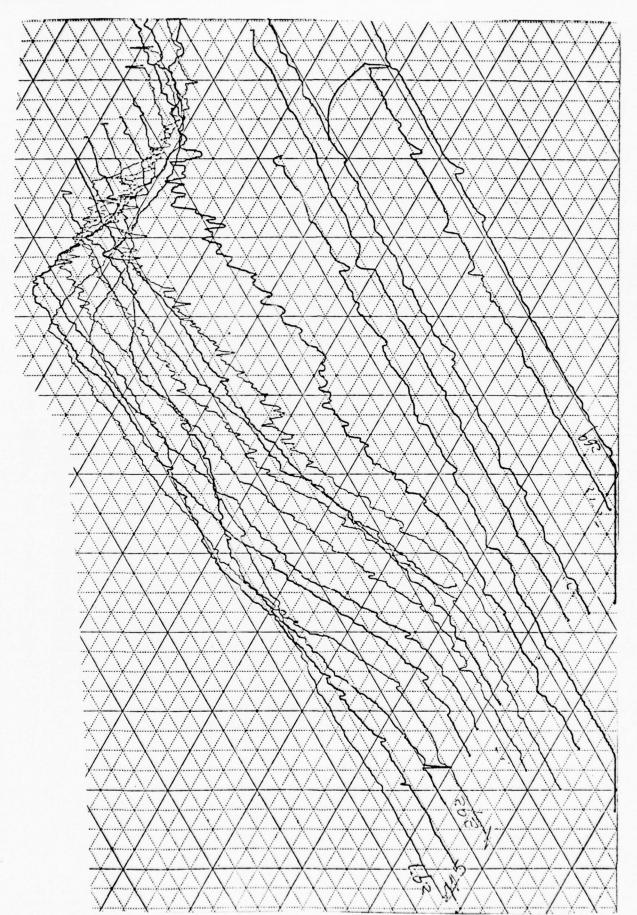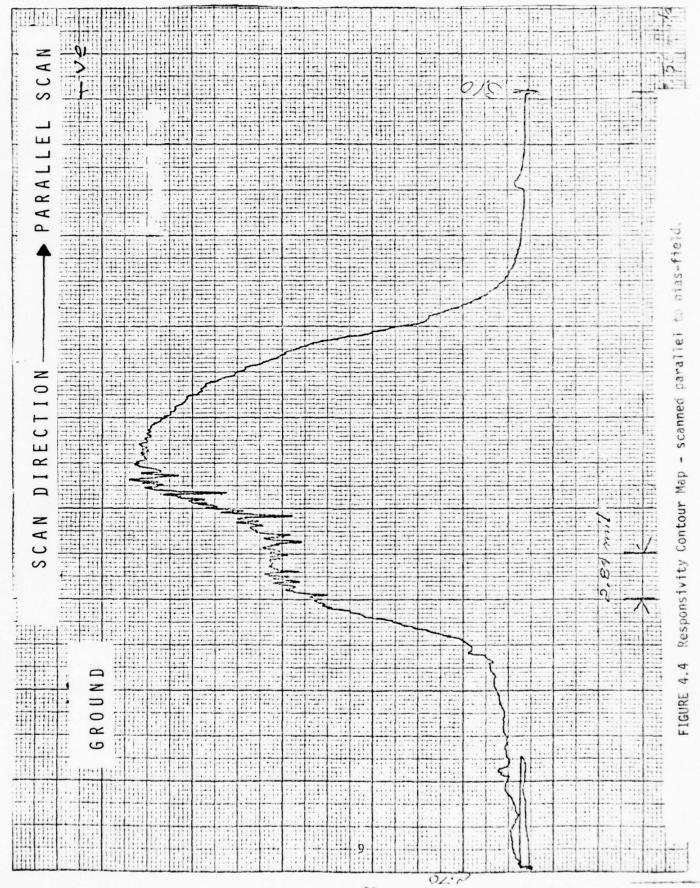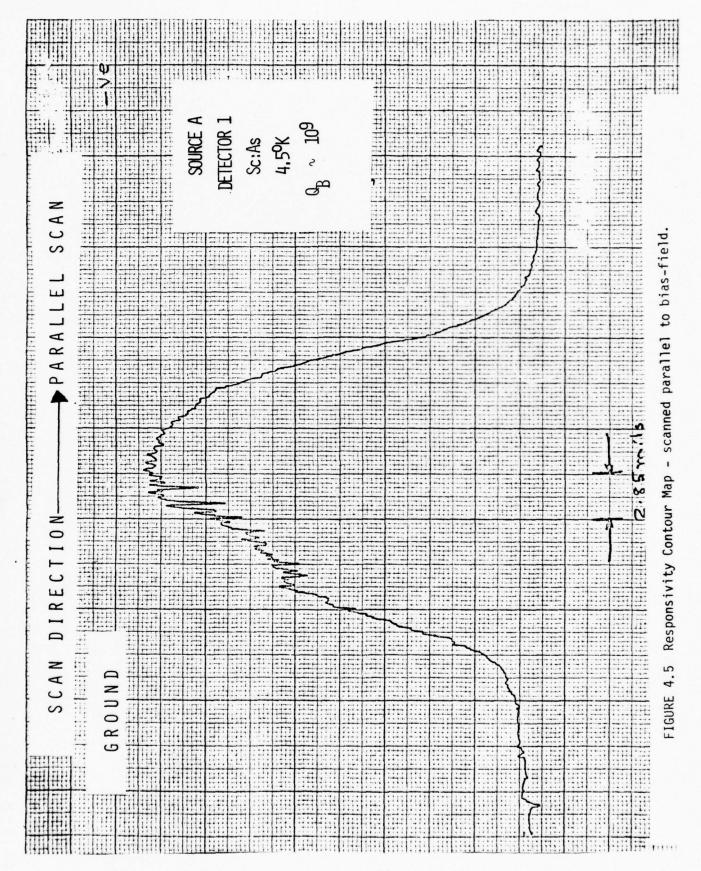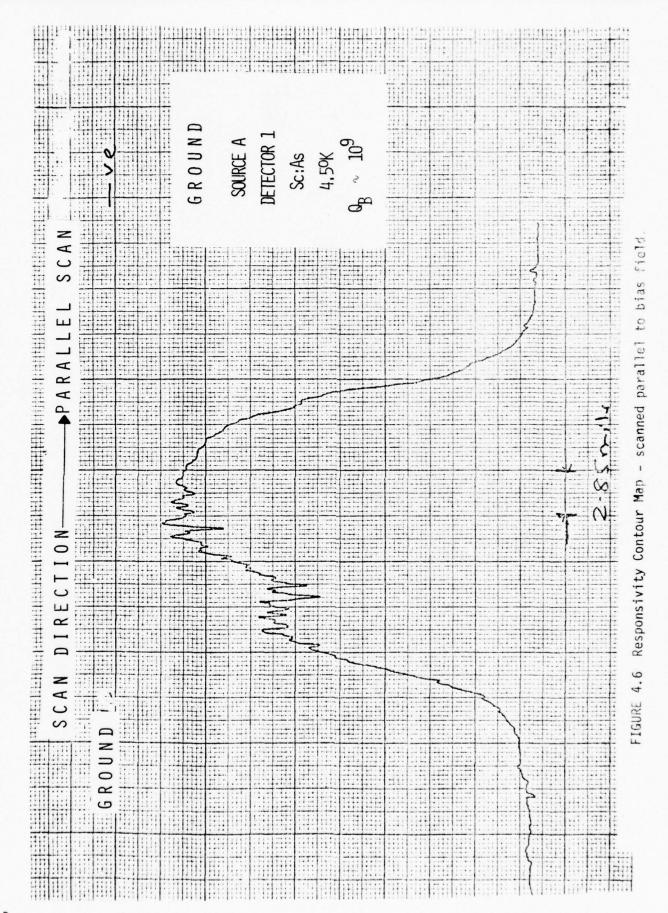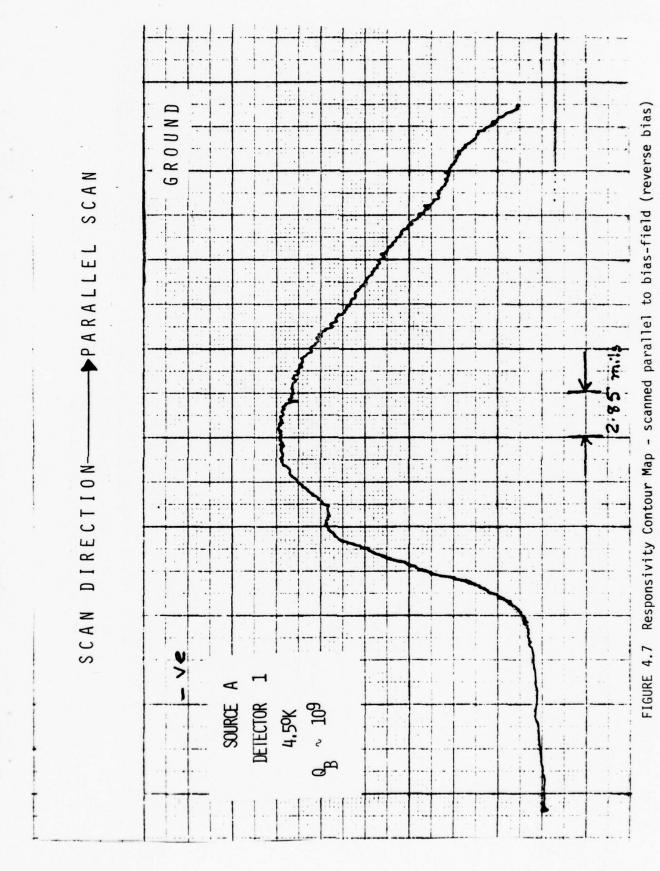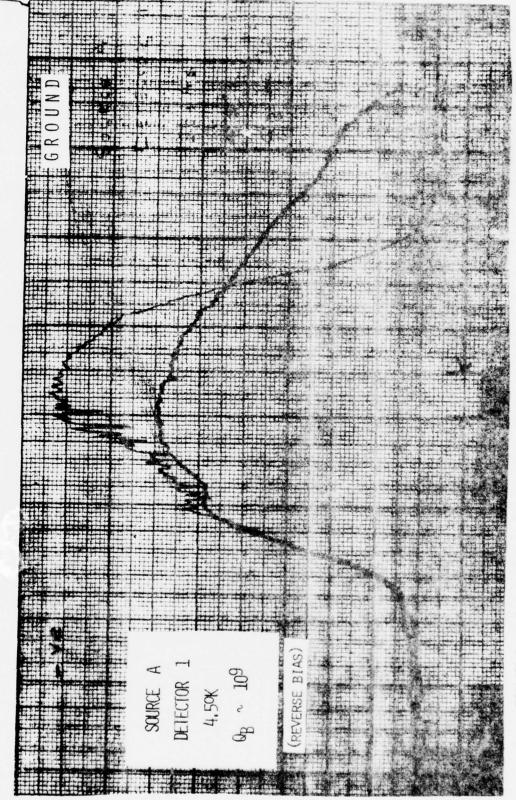
FIGURE 4.3 Pseudo - Three dimensional Responsivity Contour Map of Rockwell International Detector.

FIGURE 4.4 Responsivity Contour Map - scanned parallel to bias-field.

FIGURE 4.5 Responsivity Contour Map – scanned parallel to bias-field.

39

FIGURE 4.6 Responsivity Contour Map - scanned parallel to bias field.

FIGURE 4.7 Responsivity Contour Map - scanned parallel to bias-field (reverse bias)

41

GROUND

SOURCE A
DETECTOR 1
4.50K
$Q_B \sim 10^9$

(REVERSE BIAS)

FIGURE 4.8 Responsivity Contour Maps of Figure 4.4 and 4.7 superimposed, showing no dependance of the initial part of the contour map on the direction of the bias-field.

42

FIGURE 4.9 Responsivity Contour Map - scanned perpendicular to bias-field.

SCAN DIRECTION ➔ (PERPENDICULAR SCAN)

SOURCE A
DETECTOR 1
Si:As
4.5°K
$Q_B \sim 10^9$
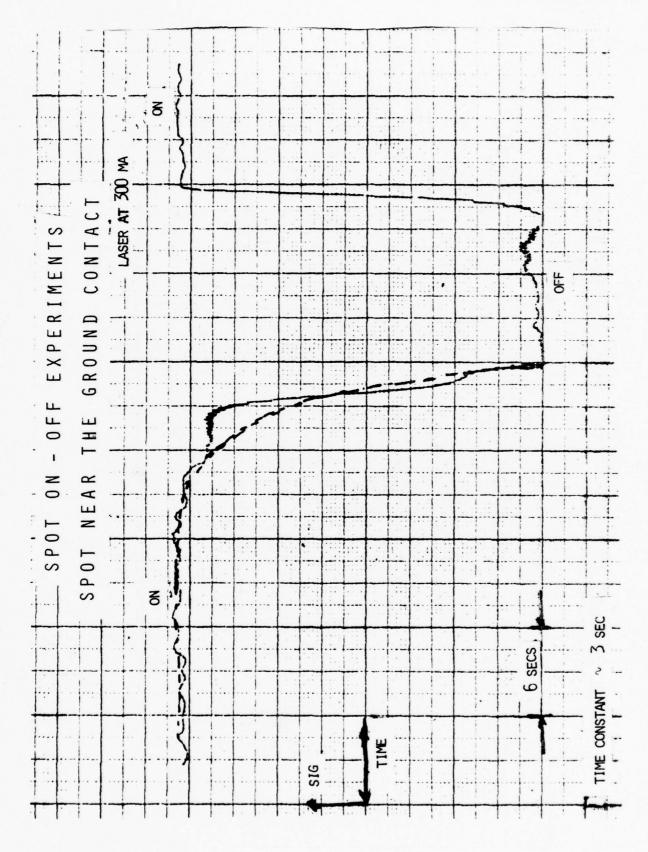
Figure 4.10. Laser Spot "On-Off" Experiment - Spot Near Ground Contact

44
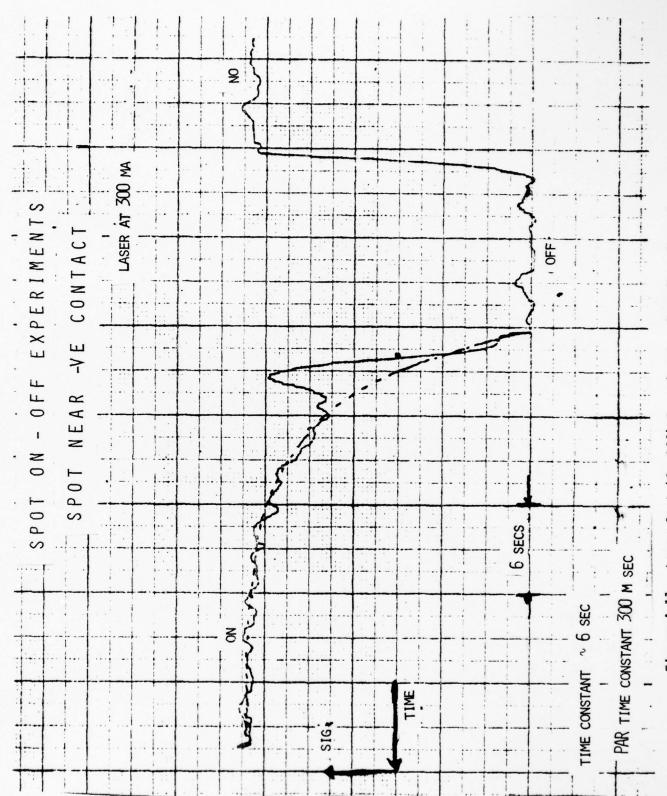
Figure 4.11. Laser Spot 'On-Off' Experiment – Spot Near Negative Contact

FIGURE 4.12

Peak Laser Current   300   ma

Modulation Frequency   1.5   Hz

Scan Speed   4.25   μm/s

Detector Bias   - 4.2   V

Amp. Setting   10

Par F.S.   200   mV

46

FIGURE 4.13

Peak Laser Current	300	ma
Modulation Frequency	1.5	Hz
Scan Speed	4.25	μm/sec
Detector Bias	- 4.2	V
Amp. Setting	5	
Par F.S.	200	mV

47

FIGURE 4.14

Peak Laser Current	300	ma
Modulation Frequency	0.5	Hz
Scan Speed	4.25	μm/sec
Detector Bias	- 4.2	V
Amp. Setting	50	
Par F.S.	500	mV

FIGURE 4.15

Peak Laser Current	300	ma
Modulation Frequency	0.5	Hz
Scan Speed	4.25	μm/sec
Detector Bias	- 4.2	V
Amp. Setting	50	
Par F.S.	500	mV

49
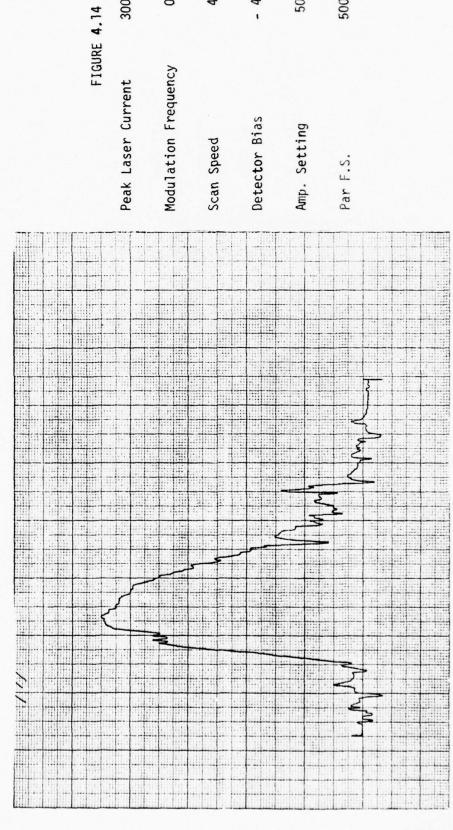
FIGURE 4.16

Peak Laser Current	300	ma
Modulation Frequency	10	Hz
Scan Speed	4.25	μm/sec
Detector Bias	- 4.2	V
Amp. Setting	50	
Par F.S.	500	mV

FIGURE 4.17

Peak Laser Current	300	ma
Modulation Frequency	1.5	Hz
Scan Speed	5.5	µm/sec
Detector Bias	- 4.2	V
Amp. Setting	5	
Par F.S.	200	mV

FIGURE 4.18

Peak Laser Current	300	ma
Modulation Frequency	1.5	Hz
Scan Speed	7.0	μm/sec
Detector Bias	- 4.2	V
Amp. Setting	5	
Par F.S.	200	mV

FIGURE 4.19

Peak Laser Current	300	ma
Modulation Frequency	5.0	Hz
Scan Speed	5.5	μm/sec
Detector Bias	- 4.2	V
Amp. Setting	50	
Par F.S.	500	mV

FIGURE 4.20

Peak Laser Current	300	ma
Modulation Frequency	5.0	Hz
Scan Speed	7.0	μm/sec
Detector Bias	- 4.2	V
Amp. Setting	50	
Par F.S.	500	mV

54

FIGURE 4.21

Peak Laser Current	300	ma
Modulation Frequency	10.0	Hz
Scan Speed	5.5	μm/sec
Detector Bias	- 4.2	V
Amp. Setting	50	
Par F.S.	500	mV

FIGURE 4.22

Peak Laser Current	300	ma
Modulation Frequency	10	Hz
Scan Speed	7.0	µm/sec
Detector Bias	- 4.2	V
Amp. Setting	50	
Par F.S.	500	mV

FIGURE 4.23

Peak Laser Current	500	ma
Modulation Frequency	5	Hz
Scan Speed	5.5	µm/sec
Detector Bias	- 4.2	V
Amp. Setting	10	
Par F.S.	200	mV

FIGURE 4.24

Peak Laser Current	500	ma
Modulation Frequency	5	Hz
Scan Speed	5.5	μm/sec
Detector Bias	- 4.2	V
Amp. Setting	10	
Par F.S.	500	mV

58
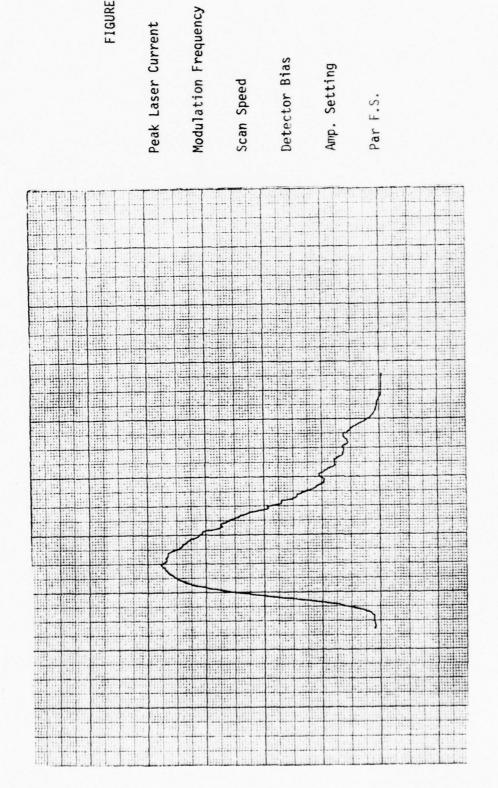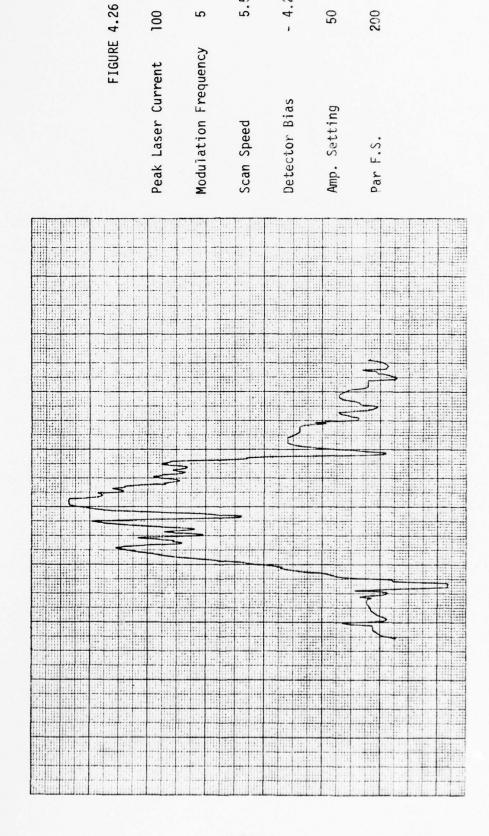
FIGURE 4.25

Peak Laser Current   100   ma

Modulation Frequency   5   Hz

Scan Speed   5.5   μm/sec

Detector Bias   - 4.2   V

Amp. Setting   50

Par F.S.   500   mV

FIGURE 4.26

Peak Laser Current	100	ma
Modulation Frequency	5	Hz
Scan Speed	5.5	μm/sec
Detector Bias	- 4.2	V
Amp. Setting	50	
Par F.S.	200	mV

60

FIGURE 4.27

Peak Laser Current	550	ma
Modulation Frequency	5	Hz
Scan Speed	5.5	µm/sec
Detector Bias	– 4.2	V
Amp. Setting	1	
Par F.S.	500	mV

61

FIGURE 4.28
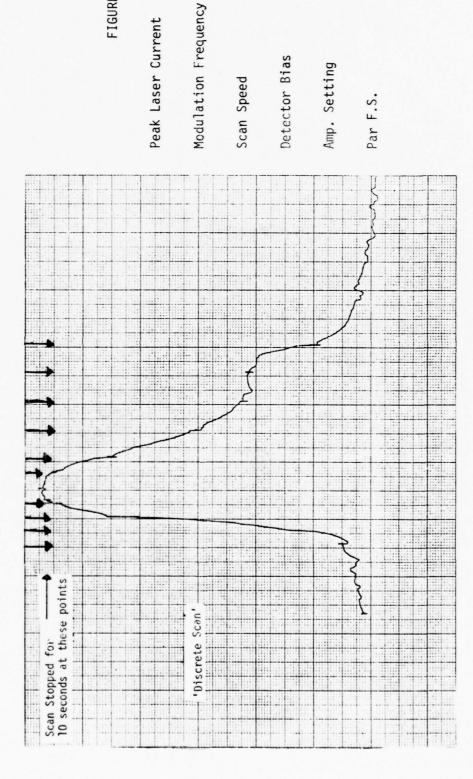
Peak Laser Current	400	ma
Modulation Frequency	5	Hz
Scan Speed	--	µm/sec
Detector Bias	- 4.2	V
Amp. Setting	10	
Par F.S.	500	mV

'Discrete' Scan

Initial Part of Contour ONLY

Scan Stopped for 10 Seconds at These Points

62

FIGURE 4.29

Peak Laser Current	400	ma
Modulation Frequency	5	Hz
Scan Speed	--	μm/sec
Detector Bias	- 4.2	V
Amp. Setting	5	
Par F.S.	500	mV

Scan Stopped for
10 seconds at these points

'Discrete Scan'
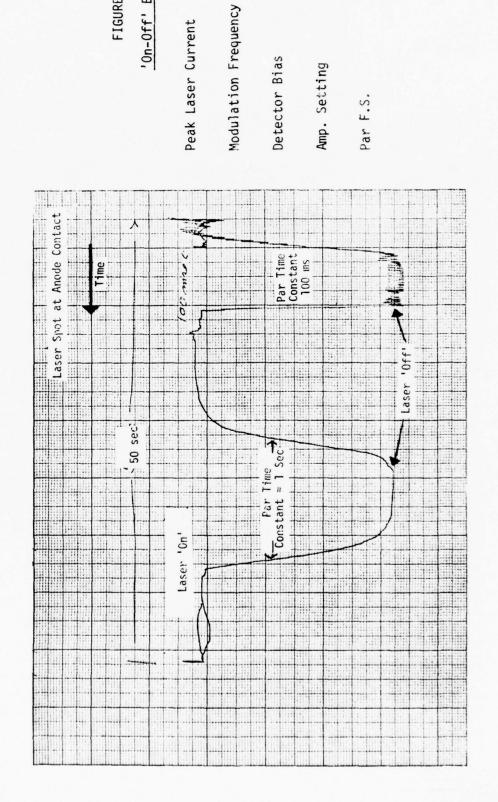
FIGURE 4.30

'On-Off' Experiment

Peak Laser Current	400	ma
Modulation Frequency	5	Hz
Detector Bias	- 4.2	V
Amp. Setting	5	
Par F.S.	500	mV

64

FIGURE 4.31

'On-Off' Experiment

Peak Laser Current	400	ma
Modulation Frequency	5	Hz
Detector Bias	- 4.2	V
Par F.S.	500	mV
Par Time Constant	100	msec

Laser 'On'

Laser 'Off'

Time

Laser Spot at the Center of Detector

65

FIGURE 4.32

Laser 'On-Off' Experiment

Peak Laser Current	400	ma
Modulation Frequency	5	Hz
Detector Bias	- 4.2	V
Amp. Setting	5	
Par F.S.	500	mV
Par Time Constant	100	m/sec

Laser Spot at Cathode

FIGURE 4.33

Peak Laser Current	1000	ma
Modulation Frequency	1.5	Hz
Scan Speed	4.25	μm/sec
Detector Bias	- 4.2	V
Amp. Setting	100	
Par F.S.	200	mV

FIGURE 4.34

Peak Laser Current   1000   ma

Modulation Frequency   1.5   Hz

Scan Speed   5.5   um/sec

Detector Bias   - 4.2   V

Amp. Setting   100

Par F.S.   200   mV

Par Q   20

Noise Spikes

FIGURE 4.35

Peak Laser Current   1000   ma

Modulation Frequency   1.5   Hz

Scan Speed   7.0   μm/sec

Detector Bias   - 4.2   V

Amp. Setting   100

Par F.S.   200   mV

Par Q   100

Noise Spikes

FIGURE 4.36

Peak Laser Current   1000   ma

Modulation Frequency   5   Hz

Scan Speed   4.25   µm/sec

Detector Bias   - 4.2   V

Amp. Setting   100

Par F.S.   200   mV

70

FIGURE 4.37

Peak Laser Current	1000	ma
Modulation Frequency	5	Hz
Scan Speed	5.5	µm/sec
Detector Bias	- 4.2	V
Amp. Setting	100	
Par F.S.	200	mV

FIGURE 4.38

Peak Laser Current	1000	ma
Modulation Frequency	5	Hz
Scan Speed	5.5	μm/sec
Detector Bias	- 4.2	V
Amp. Setting	100	
Par F.S.	200	mV

Noise Spikes

72

FIGURE 4.39

Peak Laser Current   1000   ma

Modulation Frequency   5   Hz

Scan Speed   7.0   µm/sec

Detector Bias   - 4.2   V

Amp. Setting   100

Par F.S.   200   mV

73

FIGURE 4.40

Peak Laser Current	1000	ma
Modulation Frequency	10	Hz
Scan Speed	4.25	μm/sec
Detector Bias	- 4.2	V
Amp. Setting	100	
Par F.S.	200	mV

74

FIGURE 4.41

Peak Laser Current   1000   ma

Modulation Frequency   10   Hz

Scan Speed   5.5   μm/sec

Detector Bias   - 4.2   V

Amp. Setting   100

Par F.S.   200   mV

Noise Spikes

FIGURE 4.42

Peak Laser Current	1000	ma
Modulation Frequency	10	Hz
Scan Speed	7.0	μm/sec
Detector Bias	- 4.2	V
Amp. Setting	100	
Par F.S.	200	mV

Noise Spikes

FIGURE 4.43

Peak Laser Current	1000	ma
Modulation Frequency	5	Hz
Scan Speed	5.5	μm/sec
Detector Bias	- 4.2	V
Amp. Setting	100	
Par F.S.	200	mV

77

FIGURE 4.44

Peak Laser Current	1000	ma
Modulation Frequency	5	Hz
Scan Speed	5.5	μm/sec
Detector Bias	- 4.2	V
Amp. Setting	100	
Par F.S.	200	mV

78

SECTION V

DISCUSSION OF RESULTS AND CONCLUSIONS

5.1 DISCUSSION OF RESULTS

Based on the results of Section IV, we can outline the following general
trends of these experiments.

1. For the low background photon flux conditions, the contour maps are,
in general, independent of the scan rate, laser chopping frequencies, and laser
power. Apparently, the general shape of the detector responsivity profile is
being observed. The decrease in the amplitude of the maximum signal with in-
crease in chopping frequency is consistent with the laser on/off time constants.

2. For higher laser intensities in experiments 1 and 2, the on/off rise-
time constants are faster and more symmetrical.

3. The on/off experiments show that the rise-time of the signal at low
background is longer than the fall time.

4. The high background results are too noisy to be very useful but do
indicate some unexplained change in the shape of the detector contours.

5.2 CONCLUSIONS

The experimental effort reported here should be examined as a very pre-
liminary step towards understanding or experimentally establish some of the
predicted abnormal behavior of extrinsic silicon infrared detectors. However,
some general conclusions can be derived on the basis of this work and are
listed below.

1. <u>Contact Effects</u> - Revisions in the application of the Ludman/Silverman
Theory* to Si:As after the contract was initiated showed the effects to be
milder by a factor of ten than originally believed. Hence, we are looking for
contact effects extending to $\sim 2\mu m$ with a $70\mu m$ spot. Given other non-ideal
effects (surface states, defects, etc.) expected near the contact region, it

79

is not surprising that no enhancement at the contacts was found. When this was realized, emphasis shifted to the establishment of contour reproducibility; in particular, whether a true "lifetime profile" is measured in this type of anode to cathode scan.

2. Some confidence in the reproducibility of the contours has been established within a range of scan rate, chopping frequency and laser power.

3. Better or sharper detector contacts are required to obtain accurate measurements of the contact effects--perhaps ion implanted n^+ contacts. A uniform detector response between the contacts would help the data analysis immensely. A smaller spot size would aid in the interpretation of the measurements.

4. Longer wavelength detectors with higher operating temperatures for which greater enhancement in responsivity due to carrier "spill-over" is expected** would provide a more significant test of the theory.

---

* Private Communication - Ludman/Silverman
** Private Communication - Ludman/Silverman

MISSION
of
Rome Air Development Center

RADC plans and conducts research, exploratory and advanced development programs in command, control, and communications (C^3) activities, and in the C^3 areas of information sciences and intelligence. The principal technical mission areas are communications, electromagnetic guidance and control, surveillance of ground and aerospace objects, intelligence data collection and handling, information system technology, ionospheric propagation, solid state sciences, microwave physics and electronic reliability, maintainability and compatibility.